Phonons Reflect Dynamic Spin-State Order in $LaCoO_3$

Alsu Ivashko,[1] Taishun Manjo,[2,3] Maximilian Kauth,[1] Yuliia Tymoshenko,[1] Adrian M. Merritt,[4] Klaus-Peter Bohnen,[1] Rolf Heid,[1] Michael Merz,[1,5] Andreas Eich,[1] John-Paul Castellan,[1,6] Alexandre Ivanov,[7] Nathaniel Schreiber,[8] Hong Zheng,[8] J. F. Mitchell,[8] Martin Meven,[9,10] Jitae T. Park,[11] Daisuke Ishikawa,[2,3] Yuiga Nakamura,[12] Alfred Q. R. Baron,[2,3] and Frank Weber[1]

[1]*Institute for Quantum Materials and Technologies, Karlsruhe Institute of Technology, 76131 Karlsruhe, Germany*
[2]*Materials Dynamics Laboratory, RIKEN SPring-8 Center, RIKEN, 1-1-1 Kouto, Sayo, Hyogo 679-5148, Japan*
[3]*Precision Spectroscopy Division, SPring-8/JASRI, 1-1-1 Kouto, Sayo, Hyogo 679-5198, Japan*
[4]*Physikalisches Institut, Karlsruhe Institute of Technology, 76021 Karlsruhe, Germany*
[5]*Karlsruhe Nano Micro Facility (KNMFi), Karlsruhe Institute of Technology, 76131 Karlsruhe, Germany*
[6]*Laboratoire Léon Brillouin (CEA-CNRS), CEA Saclay, F-91911 Gif-sur-Yvette, France*
[7]*Institut Laue-Langevin, 71 avenue des Martyrs CS 20156, 38042 Grenoble Cedex 9, France*
[8]*Materials Science Division, Argonne National Laboratory, Lemont, Illinois 60439, USA*
[9]*Institute of Crystallography, RWTH Aachen University, 52056 Aachen 52056, Germany*
[10]*Jülich Centre for Neutron Science (JCNS), Forschungszentrum Jülich GmbH at Heinz Maier-Leibnitz Zentrum (MLZ), 85748 Garching 85748, Germany*
[11]*Heinz Maier-Leibnitz Zentrum (MLZ), Technische Universität München, 85748 Garching, Germany*
[12]*Diffraction and Scattering Division, SPring-8/JASRI, 1-1-1 Kouto, Sayo, Hyogo 679-5198, Japan*

(Received 23 January 2026; accepted 7 August 2026; published 11 September 2026)

We investigate lattice dynamics in $LaCoO_3$ using inelastic neutron and x-ray scattering over $T = 2 - 650$ K, spanning the spin-state crossover at $T_1 \approx 100$ K and the insulator-metal transition at $T_2 \approx 550$ K. Comparison with quasiharmonic *ab initio* lattice-dynamical calculations helps reveal anomalous softening of a ≈ 10-meV oxygen phonon, confined to the temperature interval $T_1 \leq T \leq T_2$ and localized in momentum space at $\mathbf{q}_{SSO} = (½, ½, ½)_c$. This wave vector is characteristic of the spin-state-ordering pattern originally proposed by Goodenough [An interpretation of the magnetic properties of the perovskite-type mixed crystals $La_{1-x}Sr_xCoO_{3-\lambda}$, J. Phys. Chem. Solids **6**, 287 (1958)]. Our results provide momentum-resolved evidence for dynamic correlations of high-spin and low-spin Co^{3+} states characterized by $\mathbf{q}_{SSO} = (½, ½, ½)_c$, demonstrating that phonons are sensitive probes of fluctuating spin-state correlations in $LaCoO_3$.

DOI: 10.1103/tsw6-sdhk

Introduction—Spin-crossover (SCO) compounds exhibit reversible changes in electronic spin states driven by temperature, pressure, or light. They provide a model platform for studying coupled spin-lattice degrees of freedom [1–3] and are relevant to application [4,5] bistability and large entropy changes. Because spin-state transitions modify local bonding, phonons offer a particularly sensitive probe of SCO materials.

Among oxide materials, $LaCoO_3$ is a canonical example of a thermally driven SCO system: with increasing temperature, Co^{3+} ions evolve from a low-spin to higher-spin configuration, producing marked anomalies in thermal expansion [6,7], elastic moduli [8], and heat capacity [9]. Despite extensive study [10–17], the magnetic properties of $LaCoO_3$ and the temperature evolution of the Co^{3+} spin state remain debated.

At low temperature, $LaCoO_3$ adopts a slight rhombohedral distortion from the cubic symmetry of a simple perovskite [Fig. 1(a)] and magnetic susceptibility measurements [Fig. 1(b)] [18] reveal two crossover regions: a sharp one near $T_1 \approx 100$ K and a broader one near $T_2 \approx 550$ K. [Throughout the Letter, we label wave vectors with indices "c" and "rh" if they are given in the pseudocubic or rhombohedral unit cell, respectively. For more details, please see Supplemental Material (SM) [19].] These have been linked to colocalized spin-state transitions of $Co^{3+}(3d^6)$ from the low-spin (LS, t_2g^6, $S = 0$) ground state to excited intermediate-spin (IS, $t_2g^5eg^1$, $S = 1$) and high-spin (HS, $t_2g^4eg^2$, $S = 2$) states. Goodenough initially proposed [11] that, at intermediate temperatures ($T_1 \leq T \leq T_2$), where LS and HS populations are comparable, the different ionic radii of LS and

Published by the American Physical Society under the terms of the Creative Commons Attribution 4.0 International license. Further distribution of this work must maintain attribution to the author(s) and the published article's title, journal citation, and DOI.

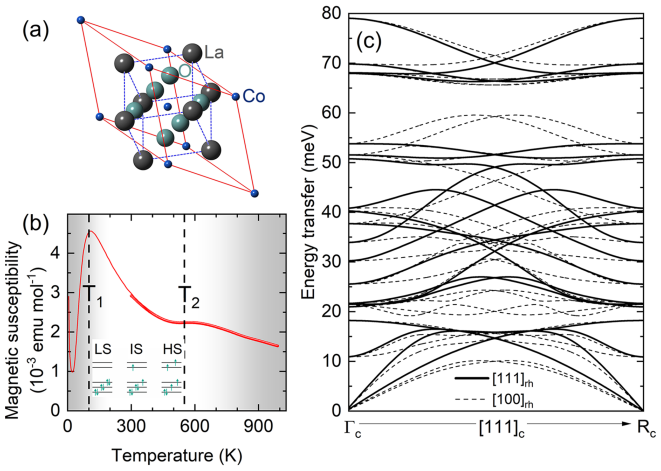

FIG. 1. (a) Pseudocubic perovskite structure of $LaCoO_3$. The red solid lines indicate the orientation of the low-temperature rhombohedral unit cell used for the phonon calculations. (b) Magnetic susceptibility of $LaCoO_3$. Data at $T \geq 300$ K were measured on our sample. Data below room temperature are taken from Ref. [18]. Dashed vertical lines denote the crossover temperatures T_1 and T_2 (see text). The inset at the bottom depicts the configuration of the $3d$ electrons of the Co^{3+} ion in the low (LS), intermediate (IS), and high spin (HS) states. (c) Calculated phonon dispersion shown for the pseudocubic $[111]_c$ direction, which corresponds to two rhombohedral directions, i.e., $[111]_{rh}$ (solid lines) and $[100]_{rh}$ in multidomain samples (dashed lines).

HS states of $Co^{3+}(r_{LS}/r_{HS} \approx 0.9)$ yield a spin-state order (SSO) consisting of sets of alternating (111) planes, in one of which the Co ions are predominantly in an HS state and in the other in an LS state. The corresponding ordering wave vector is $\mathbf{q}_{SSO} = (½, ½, ½)_c$. Although diffraction experiments found no evidence of such order [35,36], indirect probes suggest LS-HS coexistence in this regime [12,14,37]. In 1995, local density approximation with Hubbard U calculations by Korotin *et al.* [38] suggested instead a substantial IS population, implying orbital order (OO) of Co e_g orbitals with an ordering vector $\mathbf{q}_{OO} = (½, ½, 0)_c$. This IS-state scenario has since been invoked regularly to interpret experimental data [15,39,40]. More recently, the interpretation of the spin-state crossover has evolved beyond the original LS-HS versus IS dichotomy. Many-body calculations emphasize strong charge and spin fluctuations [16], while spectroscopic studies point to mobile IS excitons [41], short-range spin-state correlations [17,37], and an inhomogeneous mixed-spin-state state with spin-state-specific lattice relaxations [14]. Despite these advances, the spatial character of the associated lattice correlations remains largely unexplored.

Here, we present an investigation of lattice dynamics in $LaCoO_3$ across the temperature-driven SCO employing inelastic x-ray (IXS) and neutron scattering and extending beyond previous studies [42,43]. We use the measured phonon dispersion near the wave vectors $\mathbf{q}_{SSO}$ and $\mathbf{q}_{OO}$ as a dynamic probe of the SCO transition. We also experimentally verify the rhombohedral distortion by x-ray and neutron diffraction, using *ab initio* lattice dynamics based on density functional perturbation theory (DFPT). Quasiharmonic calculations, incorporating the reported temperature dependence of lattice constants [36], predict conventional phonon softening due to thermal expansion and, thus, help us to identify anomalous softening because of the SCO. Our main finding is softening of an oxygen-dominated low-energy phonon confined to $\mathbf{q}_{SSO} = (½, ½, ½)_c$ present only for temperatures between the spin-state and insulator-metal crossover, $T_1 \leq T \leq T_2$. This highly selective anomaly identifies the characteristic wave vector of the lattice correlations associated with the spin-state crossover and provides momentum-resolved evidence for a fluctuating spin-state texture in $LaCoO_3$.

Methods—Electronic and lattice-dynamical properties were calculated using density-functional theory and DFPT within the mixed-basis pseudopotential framework [44,45]. Quasiharmonic calculations, based on experimentally determined lattice constants [36], were used to capture phonon frequency shifts upon heating (see SM [19]). A single crystal was grown by the floating-zone method, yielding an ≈8 cm rod. One half was used for neutron scattering, and parts from the other for magnetization and x-ray scattering.

X-ray diffraction was carried out at BL02B1 [46] (SPring-8, Japan), and complementary neutron diffraction at the HEiDi diffractometer [47] (Maier-Leibnitz Zentrum, Germany). Lattice dynamics were studied with meV-resolution IXS at BL43LXU [49,50] (SPring-8) using 21.747 keV photons [Si(11 11 11) backscattering, ∼1.4 meV resolution] and a two-dimensional analyzer array enabling simultaneous access to multiple momentum transfers (see Ref. [50] for more details of the current setup). Neutron triple-axis spectrometry was performed on the spectrometers 1 T (Laboratoire Léon Brillouin), IN8 [51,52] (Institut Laue-Langevin), and PUMA [53] (Maier-Leibnitz Zentrum) with fixed final energy of 14.7 meV and pyrolytic graphite filtering. The crystal was aligned in the $[110]_c - [001]_c$ plane and mounted in closed-cycle or liquid-helium cryofurnaces, enabling measurements up to 650 K. Energy scans were performed at constant $\mathbf{Q} = \boldsymbol{\tau} + \mathbf{q}$, with $\boldsymbol{\tau}$ a reciprocal lattice vector and $\mathbf{q}$ the phonon wave vector in the first Brillouin zone.

Results—$LaCoO_3$ features a rhombohedrally distorted perovskite structure ($R\bar{3}c$, No. 167) for temperatures below 1600 K. [54] Several neutron and x-ray diffraction studies reported no further structural changes on cooling [15,35,36]. One report however suggested a monoclinic distortion [40] ($I2/a$, No. 15), claiming that previous powder diffraction experiments could have easily missed it. Subsequent analysis of neutron powder diffraction [55] did not confirm a monoclinic distortion and set a small

upper boundary. To clarify this question, we performed synchrotron-based state-of-the-art single crystal x-ray diffraction ($T = 150 - 400$ K), and complementary single-crystal neutron diffraction ($T = 2 - 600$ K). Here, we report that all of our data can be well-described in the rhombohedral structure ($R\bar{3}c$, No. 167) (see Ref. [19] for more details). The analysis of x-ray diffraction data excludes a monoclinic distortion in our sample as is corroborated by neutron diffraction revealing a normal behavior of the oxygen thermal atomic displacement parameters with temperature (see SM [19]).

Lattice-dynamical calculations are essential for $LaCoO_3$, where the rhombohedral lattice distortion generates a highly complex phonon spectrum with up to 60 branches, e.g., along $[111]_c$ which corresponds simultaneously to $[111]_{rh}$ and $[100]_{rh}$ in a multidomain sample [Fig. 1(c)]. Our *ab initio* approach reproduces not only dispersions but also momentum- and energy-resolved phonon intensities, enabling direct comparison with IXS spectra. At the R point, $\mathbf{Q} = (2.5, 2.5, 2.5)_c$, the measured spectrum agrees with the calculated one-phonon contribution, provided a two-phonon background [56,57] is included [Fig. 2(a)]. We found that the small x-ray beam (~50 μm) probes a single domain, reducing the problem to one rhombohedral vector, $\mathbf{Q} = (5, 5, 5)_{rh}$, where only four phonons carry finite intensity—greatly simplifying the analysis. Measurements centered at $\mathbf{Q} = (2.5, 2.5, 2.5)_c$ and $\mathbf{Q} = (0.5, 3.5, 3.5)_c$ [Figs. 2(b) and 2(c)] confirm this picture. The good agreement between calculated and observed intensities corroborates the calculated phonon eigenvectors. For instance, the high-energy mode near 70 meV is absent at the former and present at the latter wave vector, in agreement with single domain calculations. These high-energy Co-O breathing-type modes, extensively studied in cuprates [58–61] and manganites [62,63], show no anomalous behavior at finite momentum transfers except for a general suppression of spectral weight on heating (see SM [19]). Phonons at intermediate energies of 40–45 meV, however, display an intriguing opposite trend in their temperature dependent energies (see SM [19]) which we will further investigate and report on at a later time. Here, we focus on the phonon near 10 meV visible at $\mathbf{Q} = (0.5, 3.5, 3.5)_c$ [Fig. 2(c)], which shows anomalous softening and broadening at elevated temperatures as shown below. While the initial softening can be followed by x-ray spectroscopy [see Fig. S3], an increasing background and low phonon intensities do not allow a detailed analysis at high temperatures. Low x-ray scattering intensities of the 10-meV mode originate in its displacement pattern, or eigenvector, which is dominated by oxygen motions (see below). In the following, we investigated this phonon by inelastic neutron scattering because of the mass dependence of x-ray scattering intensities. At $\mathbf{Q} = (1.5, 1.5, 1.5)_c$ and $(1.5, 1.5, 2.5)_c$ [Figs. 3(a) and 3(b)], the 10-meV mode [64] exhibits strong softening with increasing temperature and linewidth broadening near T_1, while no

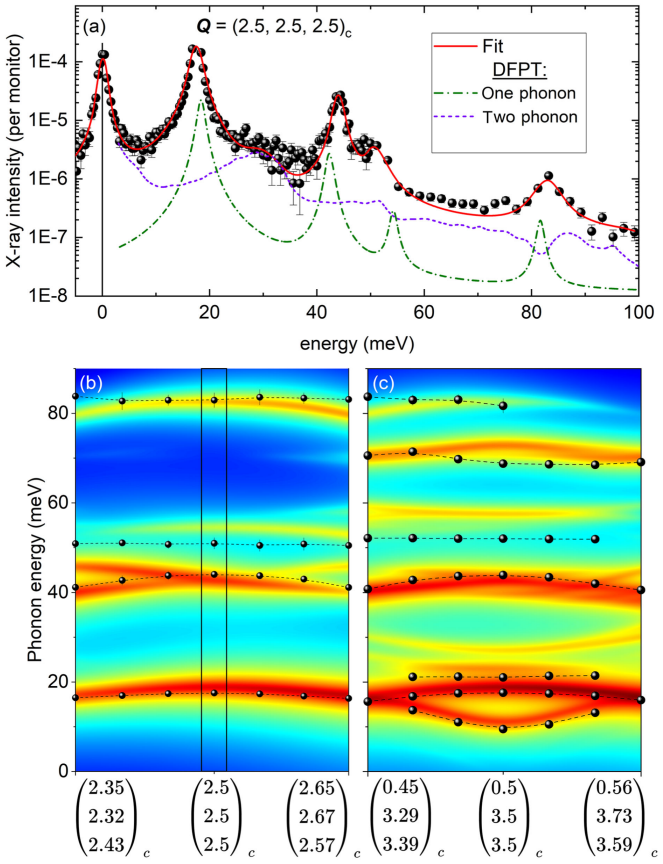

FIG. 2. (a) Inelastic x-ray scattering data taken at T = 100 K and $\boldsymbol{Q} = (2.5, 2.5, 2.5)_c [\equiv (5, 5, 5)_{rh}]$. The fit (red, solid line) consists of damped harmonic oscillator peaks for one-phonon excitations (convoluted with the experimental resolution) on top of a two-phonon background (purple, short-dashed) estimated from our DFPT calculations and the code presented in [57]. Calculated one-phonon intensities are shown as green dash-dotted line (includes a constant background of 10^{-8} for visibility) and represent single-domain spectra for the above given rhombohedral wave vector $\boldsymbol{Q} = (5, 5, 5)_{rh}$ (see text for more details). We note the relative intensity of the one- and two-phonon calculations is *not* free, so the agreement is excellent. (b),(c) Color-coded calculated intensities (log. scale: red, high; blue, low) for wave vectors probed by the horizontal row of seven IXS analyzers and detectors when the main analyzer or detector is set to (b) $\boldsymbol{Q} = (2.5, 2.5, 2.5)_c$ and (c) $(0.5, 3.5, 3.5)_c$ (see Ref. [50] for more details of the setup). Symbols denote observed phonon energies. The box in (b) marks the position for which data are shown in panel (a). Calculations presented in this figure used energies scaled by a factor of 1.03 providing the best average agreement with the experimental results (see text).

anomaly is found for the low-energy phonon branch dispersing at $\mathbf{Q} = (1.6, 1.6, 1.6)_c$ [Fig. 3(c)] or in higher-energy modes at the R point [Fig. 3(b)]. Similarly, the lowest-energy modes at the M point, $\mathbf{Q} = (1.5, 2.5, 0)_c$, show no particularly strong softening or broadening [Fig. 3(d)]. The strong softening and broadening are confirmed by subsequent measurements (see SM [19]).

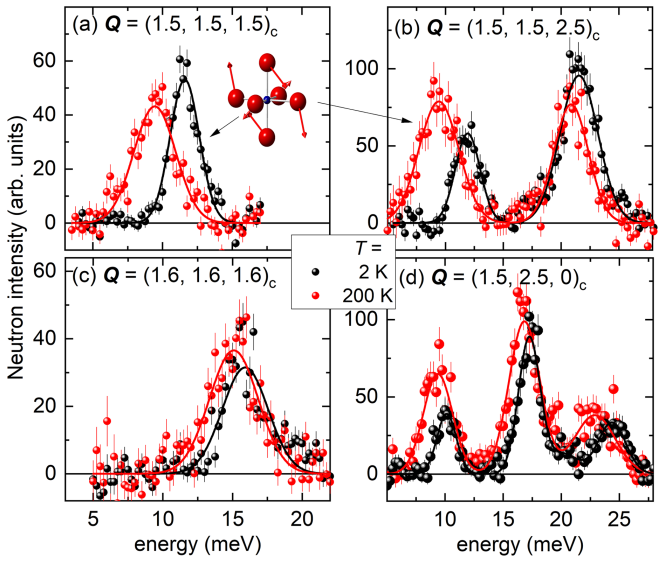

FIG. 3. Inelastic neutron scattering data at two R points, (a) $\boldsymbol{Q} = (1.5, 1.5, 1.5)_c$ and (b) $\boldsymbol{Q} = (1.5, 1.5, 2.5)_c$, (c) slightly off the R point at $\boldsymbol{Q} = (1.6, 1.6, 1.6)_c$, and (d) the M point at $\boldsymbol{Q} = (1.5, 2.5, 0)_c$ for temperatures T = 2 K (black symbols) and 200 K (red symbols). A linear background has been subtracted. Lines denote Gaussian fits. The inset in panel (a) shows the calculated displacement pattern of the 10-meV mode at the R point. Note that the scattering intensities near 10 meV measured at $\boldsymbol{Q} = (1.5, 1.5, 1.5)_c$ and $\boldsymbol{Q} = (1.5, 1.5, 2.5)_c$ represent the same phonon mode.

Quasiharmonic calculations, which reproduce most phonon energies, fail to capture this effect [Figs. 4(a) and 4(b)]: the 10-meV mode at the R point softens well below the quasiharmonic prediction between $T_1 \approx 100$ K and $T_2 \approx 550$ K, before converging with theory at higher temperatures (red symbols). This anomalous renormalization is absent for the phonon measured at $\mathbf{Q} = (1.6, 1.6, 1.6)_c$ [solid black symbols in Fig. 4(a)], in the higher-energy mode at the R point [open black symbols in Fig. 4(b)] as well as at the M point [solid blue symbols in Fig. 4(b)] [65]. The observed temperatures dependences for these modes agree well with the corresponding quasiharmonic predictions (see color-coded solid and dashed lines in corresponding figures). Taken together with the absence of additional anomalous softening in our IXS data, we argue that anomalous softening is restricted to the oxygen phonon at the cubic R point in $LaCoO_3$. We further observe that the experimentally observed linewidths of the 10-meV modes at the R [red symbols in Fig. 4(c)] and M points [blue symbols in Fig. 4(c)] are very similar at low temperatures but the R point mode acquires an additional broadening just below the crossover temperature T_1 not observed for the M point mode.

The temperature dependence of the anomalous phonon softening closely parallels that of the reported paramagnetic scattering intensity measured by polarized neutron scattering [66] (Fig. 5). While the latter probes magnetic correlations and the former reflects the phonon self-energy, the similarity of their temperature dependences suggests a common origin in the spin-state crossover. Although the present measurements do not establish a quantitative microscopic relation, the confinement of the anomaly to $\mathbf{q}_{SSO} = (½, ½, ½)_c$ together with its temperature evolution strongly suggests that spin-state fluctuations contribute to the observed phonon renormalization.

Discussion—Our results agree with previous phonon investigations as far as similar regions of momentum and energy space as well as temperature were probed. However, most Raman studies did not go beyond room temperature [1,67], similar to a neutron scattering study that was limited to 200 K [42]. IXS studies [43,68] exclude the (rhombohedral) zone center and, thereby, the

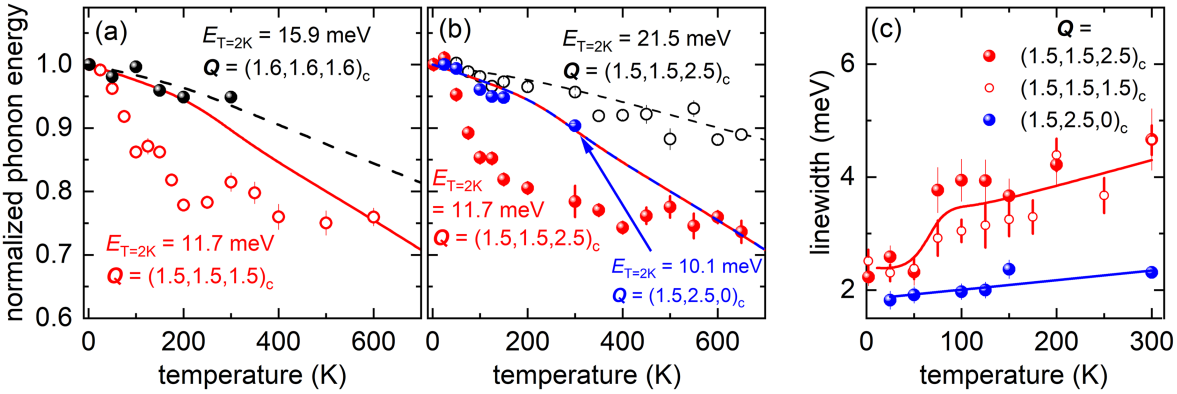

FIG. 4. (a),(b) Temperature dependent energies, normalized at T = 2 K, of phonon peaks (symbols) observed at (a) $\boldsymbol{Q} = (1.5, 1.5, 2.5)_c$ (red symbols), $\boldsymbol{Q} = (1.6, 1.6, 1.6)_c$ (black symbols), and (b) $\boldsymbol{Q} = (1.5, 1.5, 2.5)_c$ (red and black symbols), $\boldsymbol{Q} = (1.5, 2.5, 0)_c$ (blue symbols). Color-coded red, black, and blue lines in (a) and (b) are predictions for the expected phonon softening due to thermal expansion from quasiharmonic calculations (see text). (c) Experimentally observed linewidths of the lowest-energy phonon modes at $\boldsymbol{Q} = (1.5, 1.5, 2.5)_c$ (red dots), $\boldsymbol{Q} = (1.5, 1.5, 2.5)_c$ (red circles), and $\boldsymbol{Q} = (1.5, 2.5, 0)_c$ (blue dots). Color-coded lines in (c) are guides to the eye.

pseudocubic R point. In fact, the 10-meV mode at the M point was investigated by IXS [68] and was found to feature no anomalous behavior, in agreement with our findings [Figs. 3(d), 4(b), and4(c)]. Apart from these limitations, all previous studies lacked detailed lattice-dynamical calculations. In particular, quasiharmonic modelling is an indispensable tool [69]. Since we used experimentally observed lattice constants, our quasiharmonic predictions for the softening include the anomalous change of the unit-cell volume of up to 2% at T = 700 K [36,66] and our results may, thus, even underestimate the anomalous softening, $\Delta E = E_{DFPT} - E_{exp}$, by a few percent [Fig. 5].

Because the SCO alters Co-O bonding and octahedral stiffness, a comparison of our results with spin-state models in $LaCoO_3$ is revealing. The LS-HS scenario originally proposed by Goodenough [11,35,70] predicts a spin-state order consisting of alternating (111) planes enriched in HS and LS Co^{3+} ions. The different ionic radii of Co3+ in the HS and LS states increase and decrease, respectively, the size of the CoO_6 octahedron, yielding structural correlations characterized by $\mathbf{q}_{SSO} = (½, ½, ½)_c$, consistent with the observed phonon renormalization at the R point. Such correlated lattice fluctuations are expected to be strongest between T_1 and T_2, in agreement with the observed temperature dependence. Moreover, calculations identify the 10-meV mode as a predominantly oxygen vibration involving tilted rotations of the CoO_6 octahedra (inset, Fig. 5), rationalizing its strong sensitivity to spin-state-dependent lattice distortions.

Recent spectroscopic work has refined the microscopic description of the spin-state crossover in $LaCoO_3$. In

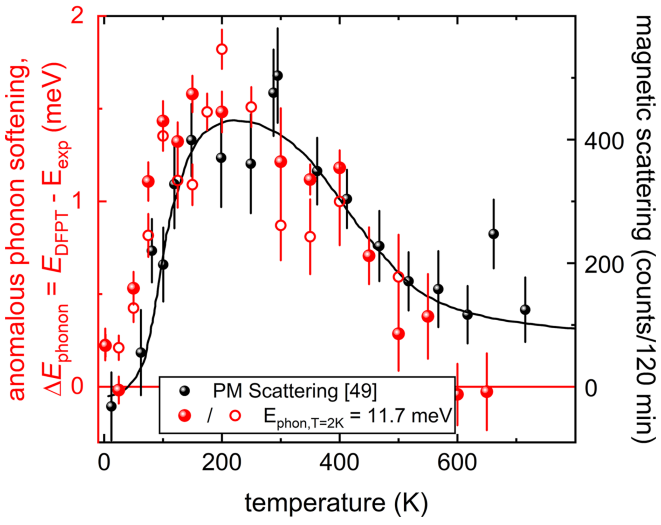

FIG. 5. Temperature dependence of the absolute anomalous softening, $\Delta E = E_{DFPT} - E_{exp}$, of the 10-meV phonon mode observed at the R point, i.e., $\boldsymbol{Q} = (1.5, 1.5, 1.5)_c$ (red-open symbols; left-hand scale) and $(1.5, 1.5, 2.5)_c$ (red-filled symbols; left-hand scale), in comparison to that of the reported paramagnetic scattering intensity (black symbols; right-hand scale) reported by Asai *et al.* [66].

particular, Takegami *et al.* [14] concluded from bulk-sensitive electron spectroscopy that paramagnetic $LaCoO_3$ is a highly inhomogeneous mixed-spin-state system consisting of coexisting LS and HS Co^{3+} sites with spin-state-specific local lattice relaxations. While Ref. [14] established the existence of local spin-state-dependent lattice distortions, the present phonon measurements provide complementary momentum-space information. The pronounced renormalization of the 10-meV phonon indicates that the associated lattice distortions possess enhanced correlations at $\mathbf{q}_{SSO} = (½, ½, ½)_c$ rather than being spatially random.

The comparison with the magnetic scattering intensity in Fig. 5 should be viewed as phenomenological rather than as a direct microscopic relation. Nevertheless, the observed anomaly exhibits the characteristic signatures of fluctuation-driven phonon renormalization known from manganites [63,71–73] and charge-density-wave materials [74–76]. In such systems the strongest anomalies occur for phonons whose eigenvectors resemble the fluctuating lattice distortion and at wave vectors corresponding to the dominant correlation vector. In $LaCoO_3$, the anomalous mode is dominated by oxygen displacements of the CoO_6 octahedra and renormalizes only near $\mathbf{q}_{SSO} = (½, ½, ½)_c$, suggesting dynamic lattice distortions associated with spin-state correlations characterized by the same wave vector.

The original IS scenario proposed by Korotin *et al.* [38] invoked orbital order of Co e_g orbitals with ordering vector $\mathbf{q}_{OO} = (½, ½, 0)_c$. The corresponding lattice distortions are expected to produce correlations at the M point and could be accommodated within a monoclinic structure [40]. However, x-ray diffraction confirms that $LaCoO_3$ remains rhombohedral and we find no phonon anomalies of the 10-meV mode at $\mathbf{q}_{OO} = (½, ½, 0)_c$ (see Figs. 3, 4, and SM), consistent with previous IXS measurements [68]. More recently, Hariki *et al.* [41] proposed an alternative description in terms of mobile IS excitons coupled to HS excitations. Our phonon measurements do not directly distinguish between local HS states, mobile IS excitons, or interacting mixtures thereof. Instead, they probe the lattice response associated with the spin-state manifold. The observation that the anomalous renormalization is confined to $\mathbf{q}_{SSO} = (½, ½, ½)_c$ and absent at $\mathbf{q}_{OO} = (½, ½, 0)_c$ demonstrates that the dominant lattice correlations possess the symmetry of the Goodenough spin-state-order pattern. Any microscopic description of the spin-state crossover, including excitonic approaches, must therefore account for this highly selective momentum dependence.

Whereas we cannot generally rule out additional phonon anomalies, our extensive measurements over a wide range of wave vectors with x-ray and neutron spectroscopy identify only the anomaly at the cubic R point. The present results therefore indicate that the dominant lattice correlations are associated with fluctuations possessing the symmetry of the Goodenough spin-state-order pattern

rather than those expected for a static IS orbital-order state, in line with several recent reports [14,16,17]. Individual phonon eigenvectors can provide enhanced sensitivity and promote highly selective renormalization effects, thereby offering a powerful route for investigating fluctuating order in correlated materials.

Summary—In summary, we establish an anomaly in an oxygen-dominated low-energy phonon in $LaCoO_3$ that is confined to the R point and present only between the spin-state and insulator-metal crossovers. The highly selective renormalization of this mode reveals dynamic lattice correlations characterized by $\mathbf{q}_{\mathrm{SSO}} = (½, ½, ½)_c$ and provides momentum-resolved evidence for the spatial organization of the spin-state manifold in $LaCoO_3$ consistent with a fluctuating LS-HS spin-state-order pattern of the type originally proposed by Goodenough [11,35,70]. More broadly, our results demonstrate that phonons can serve as sensitive probes of fluctuating order even when the associated correlations remain dynamic and below the detection limit of diffraction.

Acknowledgments—We wish to thank D. Phelan, S. Rosenkranz, and R. Osborn for helpful discussions. The work of Y. T. was supported by the consortium DAPHNE4NFDI in the context of the work of the NFDI e.V. The consortium is funded by the Deutsche Forschungsgemeinschaft (DFG, German Research Foundation)—Project No. 460248799. The work of A. M. M. was supported by BMBF, Germany, in the framework of ErUM-Pro (Projects No. 05K22VK1 and No. NMO4PUMA). Work in the Materials Science Division of Argonne National Laboratory (crystal growth, magnetic characterization) was supported by the U.S. Department of Energy, Office of Science, Basic Energy Sciences, Materials Science and Engineering Division. Parts of the presented data were measured on the single crystal diffractometer HEiDi jointly operated by RWTH Aachen University and JCNS/Forschungszentrum Jülich at the MLZ within the JARA initiative. The IXS experiments were performed at the RIKEN Quantum NanoDynamics Beamline, BL43LXU, with approval of RIKEN SPring-8 Center (Proposal No. 20220075). Neutron scattering beam time at the ILL was provided under Proposal No. 7-01-586 [52].

Data availability—Results of the crystallographic refinements and some of the data used to create Figs. 1–5 can be accessed online [48].

[1] A. Ishikawa, J. Nohara, and S. Sugai, Raman study of the orbital-phonon coupling in $LaCoO_3$, Phys. Rev. Lett. **93**, 136401 (2004).

[2] T. K. Ekanayaka, K. P. Maity, B. Doudin, and P. A. Dowben, Dynamics of spin crossover molecular complexes, Nanomater. Nanotechnol. **12**, 1742 (2022).

[3] Z. Wu and R. M. Wentzcovitch, Spin crossover in ferropericlase and velocity heterogeneities in the lower mantle, Proc. Natl. Acad. Sci. U.S.A. **111**, 10468 (2014).

[4] K. Ridier, A. Hoblos, S. Calvez, M. Lorenc, W. Nicolazzi, S. Cobo, L. Salmon, L. Routaboul, G. Molnár, and A. Bousseksou, Optical properties and photonic applications of molecular spin-crossover materials, Coord. Chem. Rev. **535**, 216628 (2025).

[5] K. Senthil Kumar and M. Ruben, Emerging trends in spin crossover (SCO) based functional materials and devices, Coord. Chem. Rev. **346**, 176 (2017).

[6] C. Zobel, M. Kriener, D. Bruns, J. Baier, M. Gruninger, T. Lorenz, P. Reutler, and A. Revcolevschi, Evidence for a low-spin to intermediate-spin state transition in $LaCoO_3$, Phys. Rev. B **66**, 020402(R) (2002).

[7] K. Berggold, M. Kriener, P. Becker, M. Benomar, M. Reuther, C. Zobel, and T. Lorenz, Anomalous expansion and phonon damping due to the Co spin-state transition in $RCoO_3$ $(R = La,$ Pr, $Nd,$ and $Eu)$, Phys. Rev. B **78**, 134402 (2008).

[8] S. Murata, S. Isida, M. Suzuki, Y. Kobayashi, K. Asai, and K. Kohn, Elastic anomalies with the spin-state transitions in $LaCoO_3$, Physica B (Amsterdam) **263–264**, 647 (1999).

[9] M. Rotter, Z.-S. Wang, A. T. Boothroyd, D. Prabhakaran, A. Tanaka, and M. Doerr, Mechanism of spin crossover in $LaCoO_3$ resolved by shape magnetostriction in pulsed magnetic fields, Sci. Rep. **4**, 7003 (2014).

[10] G. H. Jonker and J. H. v. Santen, Magnetic compounds with perovskite structure III: Ferromagnetic compounds of cobalt, Physica (Amsterdam) **19**, 120 (1953).

[11] J. B. Goodenough, An interpretation of the magnetic properties of the perovskite-type mixed crystals $La_{1-x}Sr_xCoO_{3-\lambda}$, J. Phys. Chem. Solids **6**, 287 (1958).

[12] M. W. Haverkort *et al.*, Spin state transition in $LaCoO_3$ studied using soft x-ray absorption spectroscopy and magnetic circular dichroism, Phys. Rev. Lett. **97**, 176405 (2006).

[13] Y. Tokura, Y. Okimoto, S. Yamaguchi, H. Taniguchi, T. Kimura, and H. Takagi, Thermally induced insulator-metal transition in $LaCoO_3$: A view based on the Mott transition, Phys. Rev. B **58**, R1699 (1998).

[14] D. Takegami *et al.*, Paramagnetic $LaCoO_3$: A highly inhomogeneous mixed spin-state system, Phys. Rev. X **13**, 011037 (2023).

[15] M. Feygenson *et al.*, Manifold of spin states and dynamical temperature effects in $LaCoO_3$: Experimental and theoretical insights, Phys. Rev. B **100**, 054306 (2019).

[16] M. Karolak, M. Izquierdo, S. L. Molodtsov, and A. I. Lichtenstein, Correlation-driven charge and spin fluctuations in $LaCoO_3$, Phys. Rev. Lett. **115**, 046401 (2015).

[17] Y. Shimizu, T. Takahashi, S. Yamada, A. Shimokata, T. JinNo, and M. Itoh, Symmetry preservation and critical fluctuations in a pseudospin crossover perovskite $LaCoO_3$, Phys. Rev. Lett. **119**, 267203 (2017).

[18] A. S. Panfilov, G. E. Grechnev, I. P. Zhuravleva, A. A. Lyogenkaya, V. A. Pashchenko, B. N. Savenko, D. Novoselov, D. Prabhakaran, and I. O. Troyanchuk, Pressure effect on magnetic susceptibility of $LaCoO_3$, Low Temp. Phys. **44**, 328 (2018).

[19] See Supplemental Material http://link.aps.org/supplemental/10.1103/tsw6-sdhk for more details, which includes Refs. [20–34].

[20] G. Thornton, B. C. Tofield, and A. W. Hewat, A neutron diffraction study of $LaCoO_3$ in the temperature range $4.2 < T < 1248\,K$. J. Solid State Chem. **61**, 301 (1986).

[21] D. Vanderbilt, Optimally smooth norm-conserving pseudopotentials, Phys. Rev. B **32**, 8412 (1985).

[22] J. P. Perdew and Y. Wang, Accurate and simple analytic representation of the electron-gas correlation energy, Phys. Rev. B **45**, 13244 (1992).

[23] S. Baroni, P. Giannozzi, and E. Isaev, Density-functional perturbation theory for quasi-harmonic calculations, Theor. Comput. Methods Miner. Phys. **71**, 39 (2010).

[24] A. Debernardi, M. Alouani, and H. Dreyssé, Ab initio thermodynamics of metals: Al and W, Phys. Rev. B **63**, 064305 (2001).

[25] A. A. Quong and A. Y. Liu, First-principles calculations of the thermal expansion of metals, Phys. Rev. B **56**, 7767 (1997).

[26] S. L. Chaplot, W. Reichardt, L. Pintschovius, and N. Pyka, Common interatomic potential model for the lattice dynamics of several cuprates, Phys. Rev. B **52**, 7230 (1995).

[27] W. Reichardt and M. Braden, Anomalous features in the bond stretching vibrations of $La_{1-x}Sr_xMnO_3$, Physica B (Amsterdam) **263–264**, 416 (1999).

[28] L. Pintschovius,D. Reznik, W. Reichardt, Y. Endoh, H. Hiraka, J. M. Tranquada, H. Uchiyama, T. Masui, and S. Tajima, Oxygen phonon branches in $YBa_2Cu_3O_7$, Phys. Rev. B **69**, 214506 (2004).

[29] D. Reznik and W. Reichardt, Bond-bendig and bond-stretching phonons in ferromagnetic $La_{0.7}Sr_{0.3}MnO_3$, Phys. Rev. B **71**, 092301 (2005).

[30] O. De la Peña-Seaman, R. Heid, and K. P. Bohnen, First-principles study of phonon properties in magnetic double-layer manganites, Phys. Rev. B **86**, 014301 (2012).

[31] *CrysAlis PRO* (Agilent Technologies Ltd, Yarnton, Oxfordshire, England, 2014).

[32] R. H. Blessing, Data reduction and error analysis for accurate single crystal diffraction intensities, Crystallogr. Rev. **1**, 3 (1987).

[33] G. Sheldrick, Crystal structure refinement with SHELXL, Acta Crystallogr. Sect. C **71**, 3 (2015).

[34] V. Petříček, M. Dušek, and L. Palatinus, Crystallographic computing system JANA2006: General features, Z. Kristallogr. Cryst. Mater. **229**, 345 (2014).

[35] M. A. Señarís-Rodríguez and J. B. Goodenough, $LaCoO_3$ revisited, J. Solid State Chem. **116**, 224 (1995).

[36] P. G. Radaelli and S. W. Cheong, Structural phenomena associated with the spin-state transition in $LaCoO_3$, Phys. Rev. B **66**, 094408 (2002).

[37] A. Podlesnyak, S. Streule, J. Mesot, M. Medarde, E. Pomjakushina, K. Conder, A. Tanaka, M. W. Haverkort, and D. I. Khomskii, Spin-state transition in $LaCoO_3$: Direct neutron spectroscopic evidence of excited magnetic states, Phys. Rev. Lett. **97**, 247208 (2006).

[38] M. A. Korotin, S. Y. Ezhov, I. V. Solovyev, V. I. Anisimov, D. I. Khomskii, and G. A. Sawatzky, Intermediate-spin state and properties of $LaCoO_3$, Phys. Rev. B **54**, 5309 (1996).

[39] D. Phelan *et al.*, Nanomagnetic droplets and implications to orbital ordering in $La_{1-x}Sr_xCoO_3$, Phys. Rev. Lett. **96**, 027201 (2006).

[40] G. Maris, Y. Ren, V. Volotchaev, C. Zobel, T. Lorenz, and T. T. M. Palstra, Evidence for orbital ordering in $LaCoO_3$, Phys. Rev. B **67**, 224423 (2003).

[41] A. Hariki, R.-P. Wang, A. Sotnikov, K. Tomiyasu, D. Betto, N. B. Brookes, Y. Uemura, M. Ghiasi, F. M. F. de Groot, and J. Kuneš, Damping of spinful excitons in $LaCoO_3$ by thermal fluctuations: Theory and experiment, Phys. Rev. B **101**, 245162 (2020).

[42] Y. Kobayashi, T. Sin Naing, M. Suzuki, M. Akimitsu, K. Asai, K. Yamada, J. Akimitsu, P. Manuel, J. M. Tranquada, and G. Shirane, Inelastic neutron scattering study of phonons and magnetic excitations in $LaCoO_3$, Phys. Rev. B **72**, 174405 (2005).

[43] A. Doi, J. Fujioka, T. Fukuda, S. Tsutsui, D. Okuyama, Y. Taguchi, T. Arima, A. Q. R. Baron, and Y. Tokura, Multi-spin-state dynamics during insulator-metal crossover in $LaCoO_3$, Phys. Rev. B **90**, 081109(R) (2014).

[44] B. Meyer, C. Elsässer, F. Lechermann, and M. Fähnle, *FORTRAN90 Program for Mixed-Basis Pseudopotential Calculations for Crystals* (Max-Planck-Institut für Metallforschung, Stuttgart).

[45] R. Heid and K.-P. Bohnen, Linear response in a density-functional mixed-basis approach, Phys. Rev. B **60**, R3709 (1999).

[46] K. Sugimoto *et al.*, Extremely high resolution single crystal diffractometery for orbital resolution using high energy synchrotron radiation at SPring-8, AIP Conf. Proc. **1234**, 887 (2010).

[47] M. Meven and A. Sazonov, HEiDi: Single crystal diffractometer at hot source, J. Large-Scale Res. Facil. **1**, A7 (2015).

[48] A. Ivashko *et al.*, Phonons reflect dynamic spin-state order in $LaCoO_3$, KITopen data repository, 10.35097/xayn6n5pmcvdk776 (2026).

[49] A. Q. R. Baron, Status of the RIKEN quantum nanodynamics beamline (BL43LXU): The next generation for inelastic X-ray scattering, SPring-8 Inf. News, vol. **15**, p. 14 (2010).

[50] A. Q. R. Baron, Introduction to high-resolution inelastic X-ray scattering, arXiv:1504.01098.

[51] A. Piovano and A. Ivanov, The TAS-IN8 upgrade: Towards the limit of a three-axis spectrometer performance, EPJ Web Conf. **286**, 03011 (2023).

[52] A. Gazizulina, A. Ivanov, Y. Tymoshenko, and F. Weber, in *Anomalous dispersion of Co-O breathing modes in $LaCoO_3$* (Institut Laue-Langevin (ILL), 2023), 10.5291/ILL-DATA.7-01-586.

[53] O. Sobolev and J. T. Park, PUMA: Thermal three axes spectrometer, J. Large-Scale Res. Facil. **1**, A13 (2015).

[54] Y. Kobayashi, T. Mitsunaga, G. Fujinawa, T. Arii, M. Suetake, K. Asai, and J. Harada, Structural Phase Transition from Rhombohedral to Cubic in $LaCoO_3$, J. Phys. Soc. Jpn. **69**, 3468 (2000).

[55] D. Phelan, Constraints on the possible long-range orbital ordering in $LaCoO_3$, J. Magn. Magn. Mater. **350**, 183 (2014).

[56] A. Baron, in *Synchrotron Light Sources and Free Electron Lasers*, edited by E. J. Jaeschke, S. Khan, J R Schneider, and J. B. Hastings (Springer, New York, 2015), pp. 1643–1758.

[57] A. Q. R. Baron, H. Uchiyama, R. Heid, K. P. Bohnen, Y. Tanaka, S. Tsutsui, D. Ishikawa, S. Lee, and S. Tajima, Two-phonon contributions to the inelastic x-ray scattering spectra of MgB_2, Phys. Rev. B **75**, 020505(R) (2007).

[58] T. Fukuda, J. Mizuki, K. Ikeuchi, K. Yamada, A. Q. R. Baron, and S. Tsutsui, Doping dependence of softening in the bond-stretching phonon mode of $La_{2-x}Sr_xCuO_4 (0 \leq x \leq 0.29)$, Phys. Rev. B **71**, 060501(R) (2005).

[59] D. Reznik, L. Pintschovius, M. Ito, S. Iikubo, M. Sato, H. Goka, M. Fujita, K. Yamada, G. D. Gu, and J. M. Tranquada, Electron-phonon coupling reflecting dynamic charge inhomogeneity in copper oxide superconductors, Nature (London) **440**, 1170 (2006).

[60] M. d'Astuto, G. Dhalenne, J. Graf, M. Hoesch, P. Giura, M. Krisch, P. Berthet, A. Lanzara, and A. Shukla, Sharp optical-phonon softening near optimal doping in $La_{2-x}Ba_xCuO_{4+\delta}$ observed via inelastic x-ray scattering, Phys. Rev. B **78**, 140511 (2008).

[61] Q. Wang *et al.*, Charge order lock-in by electron-phonon coupling in $La_{1.675}Eu_{0.2}Sr_{0.125}CuO_4$, Sci. Adv. **7**, eabg7394 (2021).

[62] Z. Sun *et al.*, Quasiparticlelike peaks, kinks, and electron-phonon coupling in the $(\pi, 0)$ regions in the CMR oxide $La_{2-2x}Sr_{1+2x}Mn_2O_7$, Phys. Rev. Lett. **97**, 056401 (2006).

[63] F. Weber, N. Aliouane, H. Zheng, J. F. Mitchell, D. N. Argyriou, and D. Reznik, Signature of checkerboard fluctuations in the phonon spectra of a possible polaronic metal $La_{1.2}Sr_{1.8}Mn_2O_7$, Nat. Mater. **8**, 798 (2009).

[64] The scattering intensities near 10 meV measured at $\boldsymbol{Q} = (1.5, 1.5, 1.5)_c$ and $\boldsymbol{Q} = (1.5, 1.5, 2.5)_c$ (both corresponding to rhombohedral zone-center wave vectors) represent the same phonon mode.

[65] The absolute energies of the measured phonons are available in a table attached electronically to this report.

[66] K. Asai, O. Yokokura, N. Nishimori, H. Chou, J. M. Tranquada, G. Shirane, S. Higuchi, Y. Okajima, and K. Kohn, Neutron-scattering study of the spin-state transition and magnetic correlations in $La_{1-x}Sr_xCoO_3$ (x = 0 and 0.08), Phys. Rev. B **50**, 3025 (1994).

[67] V. Gnezdilov, V. Fomin, A. V. Yeremenko, K.-Y. Choi, Y. Pashkevich, P. Lemmens, S. Shiryaev, G. Bychkov, and S. Barilo, Low-temperature mixed spin state of Co3+ in $LaCoO_3$ evidenced from Jahn-Teller lattice distortions. Low Temp. Phys. **32**, 162 (2006).

[68] V. V. Sikolenko, S. L. Molodtsov, M. Izquierdo, I. O. Troyanchuk, D. Karpinsky, S. I. Tiutiunnikov, E. Efimova, D. Prabhakaran, D. Novoselov, and V. Efimov, Correlated oxygen displacements and phonon mode changes in $LaCoO_3$ single crystal, Physica B (Amsterdam) **536**, 597 (2018).

[69] S. Krannich *et al.*, Magnetic moments induce strong phonon renormalization in FeSi, Nat. Commun. **6**, 8961 (2015).

[70] P. M. Raccah and J. B. Goodenough, First-order localized-electron to collective-electron transition in $LaCoO_3$, Phys. Rev. **155**, 932 (1967).

[71] F. Weber, D. N. Argyriou, O. Prokhnenko, and D. Reznik, Large lattice distortions associated with the magnetic transition in $La_{0.7}Sr_{0.3}MnO_3$, Phys. Rev. B **88**, 241106(R) (2013).

[72] M. Maschek, D. Lamago, J. P. Castellan, A. Bosak, D. Reznik, and F. Weber, Polaronic metal phases in $La_{0.7}Sr_{0.3}MnO_3$ uncovered by inelastic neutron and x-ray scattering, Phys. Rev. B **93**, 045112 (2016).

[73] M. Maschek, J. P. Castellan, D. Lamago, D. Reznik, and F. Weber, Polaronic correlations and phonon renormalization in $La_{1-x}Sr_xMnO_3$ (x = 0.2, 0.3), Phys. Rev. B **97**, 245139 (2018).

[74] F. Weber, S. Rosenkranz, J.-P. Castellan, R. Osborn, R. Hott, R. Heid, K.-P. Bohnen, T. Egami, A. H. Said, and D. Reznik, Extended phonon collapse and the origin of the charge-density wave in 2H-$NbSe_2$, Phys. Rev. Lett. **107**, 107403 (2011).

[75] M. Maschek, S. Rosenkranz, R. Heid, A. H. Said, P. Giraldo Gallo, I. R. Fisher, and F. Weber, Wave-vector-dependent electron-phonon coupling and the charge-density-wave transition in $TbTe_3$, Phys. Rev. B **91**, 235146 (2015).

[76] X. Shen *et al.*, Precursor region with full phonon softening above the charge-density-wave phase transition in 2*H*-$TaSe_2$, Nat. Commun. **14**, 7282 (2023).